Newcastle University e-prints

Date deposited: 16th March 2012

Version of file: Author final

Peer Review Status: Peer reviewed

Citation for item:

Further information on publisher website:

http://www.emeraldinsight.com

Publisher's copyright statement:

Use Policy:

Laser Sintering of Blended Al-Si Powders

Abstract:

Purpose - To study the effects of particle size distribution, component ratio, particle packing arrangement, and chemical constitution on the laser sintering behaviour of blended hypoeutectic Al-Si powders.

Design/methodology/approach – A range of bimodal and trimodal powder blends were created through mixing Al-12Si and pure aluminium powder. The powder blends were then processed using selective laser sintering to investigate the effect of alloy composition, powder particle size and bed density on densification and microstructural evolution.

Findings – For all of the powder blends the sintered density increases with the specific laser energy input until a saturation level is reached. Beyond this saturation level no further increase in sintered density is obtained for an increase in specific laser energy input. However, the peak density achieved for a given blend varied significantly with the chemical constitution of the alloy, peaking at approximately 9 wt% Si. The tap density of the raw powder mixture (assumed to be representative of bed density) was also a significant factor.

Originality/value – This is the first study to consider the usefulness of silicon as an alloying element in aluminium alloys to be processed by selective laser sintering. In addition the paper outlines the key factors in optimising processing parameters and powder properties in order to attain sound sinterability for direct laser sintered parts.

Keywords - Selective laser sintering (**SLS**), aluminium alloy, hypoeutectic Al-Si powders.

Paper type – Research paper

1.0 Introduction

In selective laser sintering (SLS) of metal powders, powder properties such as particle size and size distribution, component ratio, nature of particle packing arrangement, and chemical constitution play key role in the manipulation of its sintering response

(Simchi, 2006, Nakamoto *et al.,* 2009). However, literature on the effects of particle packing arrangements on the microstructure of SLS processed components is very scarce, especially related to aluminium alloy powders. In the case of steel powders research has generally addressed powder contamination issues rather than actual particle packing effects on microstructure (Niu and Chang 2000; Zhu *et al.,* 2007). Results from those studies have not been able to completely define what direct consequences the nature of particle packing arrangements has on the processing conditions, densification, and microstructure of laser sintered components.

The research reported in this paper has investigated the role of powder properties in determining the bed density, processed part density and microstructure of aluminium alloys, using blended hypoeutectic Al-12Si powders as the material for investigation. Silicon is commonly used as an alloying element for aluminium alloys which will be cast. The addition of silicon produces an alloy with a lowered melting temperature (Callister, 2007) and viscosity (Dinsdale & Quested, 2004), and both of these effects were considered to be of potential value for selective laser sintering, making it easier to generate molten material, and easier for that molten material to wet surrounding material.

2.0 Materials, Equipment and Experimental Procedure

2.1 Materials

The starting materials were powders designated as pre-alloyed Al-12Si, and pure aluminium AL-1, AL-2, AL-3, and AL-4, having varying particle sizes and distributions as outlined in Table 1. All were produced by inert gas atomisation.

The four different pure Al powders AL-1 (45-75μm), AL-2 (10-45μm), AL-3 (17-30μm), and AL-4 (10-14μm) were blended with Al-12Si at concentrations of 10wt%, 25wt%, 30wt%, 40wt%, and 50wt%. In addition four trimodal powder mixes containing 75wt% Al-12Si powder, and proportions of AL-3 and AL-4 varying between 5% to 25% were also prepared. Details of all of the powder blends are

shown in Table 2. All the blended samples were mixed in a rotational V-shaped mixer for 20 minutes at a rotational speed of 125 rpm (Olakanmi, 2008).

Powder Type	Supplier	Designation	Size Fraction (µm)
Al-12Si	ALPOCO Ltd	Al-12Si	+45 to -75
Pure Aluminium 1	ALPOCO Ltd	AL-1	+45 to -75
Pure Aluminium 2	ALPOCO Ltd	AL-2	+10 to -45
Pure Aluminium 3	Alfa Aesar	AL-3	+17 to -30
Pure Aluminium 4	Alfa Aesar	AL-4	+10 to -14

Table 1 - Particle size fractions of the aluminium
powders according to the supplier's specification

Designation	Powdered Samples	Al	Si	O	Type
I	90wt% Al-12Si + 10wt% AL-3	86.3	11.6	2.1	Bimodal
II	75wt% Al-12Si + 25wt% AL-3	89.3	8.7	2.0	Bimodal
III	50wt% Al-12Si + 50wt% AL-3	91.5	6.0	2.5	Bimodal
IV	75wt% Al-12Si + 25wt% AL-1	88.9	8.7	2.5	Bimodal
V	75wt% Al-12Si + 25wt% AL-2	89.3	8.7	2.0	Bimodal
VI	75wt% Al-12Si + 25wt% AL-4	89.5	8.6	1.9	Bimodal
VII	75% Al-12Si + 20% AL-3 +5%AL-4	89.7	8.9	1.5	Trimodal
VIII	75% Al-12Si + 15% AL-3 +10%AL-4	89.0	9.0	2.0	Trimodal
IX	75% Al-12Si + 10% AL-3 +15%AL-4	89.8	8.6	1.6	Trimodal
X	75% Al-12Si + 5% AL-3 +20%AL-4	90.2	8.5	1.3	Trimodal

Table 2 – Details of powder blends and elemental composition of powder blends by
semi-quantitative EDS analysis (wt%)

2.2 Material characterisation

A Philips XL30 ESEM Scanning Electron Microscope (SEM) with link Systems EDX and image capture accessories was employed to observe the particle shape, chemical composition and homogeneity, surface morphology and microstructure of the starting powdered samples. The as received powders are shown in Figure 1. Thereafter, a Leitz (Leica) Laborlux optical microscope, fitted with an Olympus Camedia 5050

camera digital camera and linked to a computer was used to observe the microstructure of the processed material.

Apparent and tapping densities of the aluminium powders were determined according to MPIF standards 01 (sampling metal powders), 04, and 46 (MPIF, 1995). The test for apparent density took a volume of 25 cm^3 of powder which was carefully loaded into a funnel and permitted to flow through the discharge orifice of 2.54 mm diameter and completely fill a density cup. The powder in the cup was weighed to the nearest 0.01g and its apparent density was obtained by dividing the mass of the powder by its volume. To determine the tapping density of the powders, 50g of the powder was poured into a graduated cylinder and thereafter the base of the filled cylinder was tapped squarely by hand onto a hard rubber slab until no further decrease in volume took place. The volume of the powder was read to a precision of 0.5 ml and the tap density calculated by the dividing the mass of the powder with its tapped volume. Each measurement was repeated three times with no significant variation in the apparent and tapping densities observed between repetitions, and it is the average of the three measurements which is reported.

2.3 SLS equipment and processing

All samples were produced on an experimental selective laser sintering station which has been described in full elsewhere (Hauser, 2003; Olakanmi, 2008). A Synrad 240W CO_2 laser of 0.6 mm beam diameter was used, with powders processed in an Argon atmosphere. In all cases the processing condition for each sample was repeated at least twice and the mean density value recorded. No significant variation in density between repeat tests was observed (Olakanmi, 2008).

Initial studies identified the optimum processing conditions for fabricating multiple layer parts in the Al-12Si powder alone as: laser power 200 W, scan speed 120 mm/s, layer thickness of 0.25 mm, and a scan spacing of 0.1 mm (Olakanmi, 2008). In order to have a single parameter with which to compare processing conditions it is useful to define a specific laser energy input, ψ, as;

$$\psi = \frac{P}{uhd} \qquad (1)$$

where P is the laser power (W), u the scan rate (mm/s); h the scan spacing (mm); and d the layer thickness (mm). This gives an energy input per unit volume of powder bed in J/mm^3. The developed processing conditions for the Al-12Si powders had a specific laser energy input of 67 J/mm^3, and these conditions were used as a starting point for the development of processing conditions for each powder blend.

To investigate the effect of particle size and component ratio of additive powders on the processing conditions of SLS processed hypoeutectic Al-Si powders, multiple layers were fabricated in each of the powder blends using a laser power of 200 W, scan speeds from 50 to 160 mm/s, a layer thickness of 0.25mm, and a scan spacing of 0.1 mm (producing specific laser energy inputs of 50 to 150 J/mm^3).

Samples for metallographic examination were prepared and etched in dilute Keller's reagent. Quantitative measurements of the secondary dendrite arm spacing between adjacent side of branches on the longitudinal section of a primary dendrite were made according to Gündüz and Cadirli (2002), while the volume fraction of the primary aluminium phase in the laser sintered samples was determined by the systematic point counting method because it requires the least effort per observation (as described in Gokhale (2004)). The weight fraction of the primary aluminium phase (W_α) was estimated using equation (2);

$$W_\alpha = \frac{V_\alpha \rho_\alpha}{V_\alpha \rho_\alpha + V_e \rho_e} \qquad (2)$$

where V_α is the volume fraction of the primary phase, ρ_α is the density of primary phase, W_e is the weight fraction of the eutectic phase, and ρ_e is the density of eutectic phase.

3.0 Results

3.1 Chemical Composition and Microscopic Observation of the Additive and Blended Aluminium Powders

The elemental compositions of the blended powders are shown in Table 2. All the bimodal powders and trimodal powders are designated throughout this paper as shown on the first column of Table 2.

From Figure 1, it can be seen that AL-3 and AL-4 comprised spherical particles, similar to those of Al-12Si, whereas additive powder AL-1 had both irregular and spherical particles and sample AL-2 was largely made up of irregularly shaped particles.

Figure 2 presents evidence of homogeneous mixing for various composition of blended powders when each sample was mixed for 20 minutes in the V-shape mixing device, producing blended mixes which were largely made up of spherically shaped particles. The average particle sizes of each of the starting powders estimated by SEM measurements were 65.8 μm, 62.9 μm, 35.8 μm, 23.6 μm, and 12.7 μm for Al-12Si, AL-1, AL-2, AL-3, and AL-4 respectively.

3.2 Apparent, tap, and peak sintered densities of the blended powders

The average apparent and tap densities of both the starting and the blended bimodal powders are presented in Figures 3 and 4 respectively. Figure 5 presents the apparent, tapping, and peak sintered densities of the bimodal and trimodal powder blends. The peak sintered densities of the bimodal and trimodal powders were obtained for multiple layer samples fabricated with laser power of 200 W, scan speed of 65 mm/s, layer thickness of 0.25mm, and a scan spacing of 0.1 mm (producing specific laser energy input of 125 J/mm³).

3.3 Effect of additive powders and chemical constitution on the sintered density of SLS processed blended hypoeutectic Al-Si powders

The sintered densities obtained with fixed processing conditions of 200 W laser power, 120 mm/s scan speed, layer thickness 0.25 mm and scan spacing 0.1 mm for the unblended eutectic Al-12Si and blended bimodal hypoeutectic Al-Si powders are presented in Figure 6.

3.4 Effect of particle size and component ratio of additive powders on the processing conditions of SLS processed blended hypoeutectic Al-Si powders

The average sintered density as a function of specific laser energy input, defined by equation 1, for the bimodal and trimodal blends is presented in Figure 7. The figure shows a general rise in sintered density with specific laser energy input up to a peak at 125 J/mm³, with a levelling off in sintered density beyond this. The trimodal powders show a different characteristic to the bimodal ones, with a shallower rise in density before 100 J/mm³, and a sharper rise from 100 J/mm³ to 125 J/mm³.

3.5 Effect of additive powders and chemical constitution on the microstructure of SLS processed blended hypoeutectic Al-Si powders

Polished but non-etched sections of the macrostructures and inset microstructures of SLS processed samples of Al-12Si powder blended, with additive powders of various component ratios and particle sizes are presented in Figures 8 to 12. It can be seen that changes in amount of porosity, the size and shape of pores, and the shape and coherence of the sintered structure are dependent on the change in component ratios, particle sizes of additive powders, and particle packing arrangement. In the figures, regions labelled AA represent the occurrence of melt back from one layer to another. Melt back promotes coherence in inter-particulate melting across the layers of the samples, improving the densification mechanism as well as the microstructural characteristics. Melt back had not successfully occurred in regions labelled BB where porosity is evident, reducing the sintered density.

Figure 13 shows images from optical microscope observations. The occurrence of inter-particulate diffusion, evident by the formation of necking in all the samples indicates that all samples appear to be well sintered. Agglomerate formation could be

seen to be associated with the samples containing coarse additive powders AL-1 and AL-2 (Figure 13d and e). However, Figure 13f shows that the microstructure of the blended sample 25wt% AL-4 (powder blend VI) is not optimised. Comparison of the optical macrographs and micrographs of the trimodal blended samples with the bimodal powders (Figures 8 to 13) indicates that inter-particulate bonding and coherence across the layers is declining in the following order: II > VII > VIII > VI > IV > III > IX > X > V > I. Again, evaluation of the sintered macrostructure of unblended Al-12Si (Figure 14) alongside those of the bimodal and trimodal blended powders (Figures 8 to 12) suggests that only the blended sample containing 25wt% of AL-3 (powder blend II) had an improved macrostructure.

The microstructures of the sintered blended samples revealed by etching are shown in Figures 15 to 17, with the results of the quantitative metallography are presented in Figure 18. Figures 15a, c to j confirm the occurrence of heterogeneity in the microstructure of the blended bimodal samples I, III, IV, V, and VI, and trimodal samples VII, VIII, IX, and X. In contrast, Figure 15b shows the formation of large melted regions consisting of dendrites where the 75wt% Al-12Si and 25wt% AL-3 particles (blend II) appeared to have melted homogeneously. However, Figures 16a to c and 17 a to c show that there appears to be a significant variation in the dendritic morphology from top to bottom of the SLS processed samples containing varying proportion of additive powder AL-3. The dendritic morphology at the bottom section (Figures 17 a to c) of each sintered sample appears to be coarser than that at the top section of the sample (Figures 16 a to c). Observation of etched microstructure containing 25wt% AL-3 (blend II) reveals a continuous network of finer dendrites in the sample (Figures 16b and 17b) whereas samples containing 10wt% and 50wt% AL-3 (blends I and III) have a coarser and more discontinuous network of dendrites across the depths of the samples (Figures 16a and c; 17a and c). In the case of the blended samples containing 25wt% of each of AL-1, AL-2 and AL-4 (blends VI, V and VI), the dendrite structures are noted to be coarse both at the top (Figures 16d, e, and f) and bottom (Figures 17d, e, and f) portions of the sintered samples. All the trimodal samples consist of coarse dendritic structure both at the top (Figures 16g to j) and at the bottom portions of the samples.

Figure 18 confirms the finer dendritic arm spacing of blend II, as well as showing the estimated fraction of primary aluminium dendrite phase present in the SLS processed powders.

4.0 Discussion

4.1 Bed Density

The increases in apparent and tap density seen with blending are a result of improved powder packing. The ideal packing of spheres (which assumes that all spheres are of the same diameter and that nothing inhibits the movement of spheres) results in a lattice which can be either face centre cubic or hexagonal close packed (German, 1996). The apparent density of both lattice structures is 74%. In both cases each sphere has twelve neighbours, and each sphere will be associated with three voids: one with potential to fit a smaller sphere with a diameter of 0.41 times the diameter of the primary spheres (which if achieved throughout the lattice would increase the apparent density by 5%); and two with the potential to fit a smaller sphere with a diameter of 0.22 times the diameter of the primary spheres (which if achieved throughout the lattice would increase the apparent density by 2%). This gives an approximate 5:2:1 ratio for particle diameters for use in blending powders to increase apparent or tap density, with an associated 74:5:2 wt% ratio. In practice issues of agglomeration, inter-particle friction, variations in particle size, and variations in particle shape mean that (i) ideal packing is rarely achieved, and (ii) as a result of sub-optimal packing there are more voids which smaller particles can fill.

Powder deposition in this study was via a vibrating hopper (Olakanmi, 2008), and so the tap density is considered the best indicator of bed density, although as Figure 5 shows the trends for apparent and tap density are similar. For the bimodal powders blend II has a significantly higher apparent and tap density than the Al-12Si on its own (which had a tap density of 1.72 g/cm³). This blend is 75% Al-12Si and 25% AL-3, with the ratio of their average diameters being 0.35, slightly below the 0.41 achieved from an ideal packing analysis, and the increase in tap density over Al-12Si on its own is around 11%. For the other five blends either (a) the size of the particles

9

being blended was too large (blends IV and V); (b) The size of the blends being blended was too small, perhaps causing agglomeration (blend VI); or (c) the blending ratio was different (10% AL-3 for blend I and 50% for blend III).

For the trimodal blends AL-4 was used as a smaller blending constituent, with an average diameter of 0.19 times the average diameter of the Al-12Si powders, slightly below the 0.22 indicated by the ideal packing analysis. The ratios were varied from 20% AL-3/5% AL-4 to 5% AL-3/20% AL-4 through blends VII to X and the 20% AL-3/5% AL-4 (blend VII) was the only blend to show an increased tap density over blend II, although this was a small increase ($\sim$ 3%).

Overall this suggests that the particle sizes which can be derived from a close packed sphere analysis are a useful guide for blending, as here success have been achieved with average particle sizes slightly below those predicted to be optimal, but that the volumes of the smaller constituents should be greater than close packed sphere analysis suggests, because there will be more voids in practice than the theory allows for.

4.2 Densification

Figures 6 and 7 illustrate that there are a number factors at work in determining the final density of the processed material.

- Figures 7 shows that for a particular powder blend sintered density rises with specific laser energy input until a saturation point is reached, in this case around 125 J/mm^3, beyond which increases in laser energy input do not produce further increases in density. This was also observed by Simchi (2006), Muntaz *et al.,* (2008), and Bertol *et al.,* (2010) in processing steel, waspalloy, and titanium powders respectively, and is attributed to the higher levels of energy promoting delamination (as a result of residual stresses) and porosity. It is worth noting for completeness that the specific laser energy input is not a good indicator on its own, the rate at which it is delivered is also important (so very slow scan speeds with high laser power do not give the same results as very fast scan speeds with

low laser power). However, within a defined processing window Figure 7 shows it to be a useful measure.

- Figure 6 shows that the addition of 9-12 wt% (either in a powder blend or in a pre-alloyed powder) silicon to aluminium powders increases the density by 0.5-0.6 g/cm^3, from around 55% density to around 75% density. Figures 4 and 6 show that SLS of the pure Al powders did not have produce parts with densities significantly different from the tap density of the powders, and so the addition of Si is clearly useful in processing Al alloys by SLS. From the results with between 9 wt% and 12 wt% silicon it seems that the further addition of silicon would not have any significant effect on densification.

- Figure 6 also shows a distinct peak in densification for powder mixtures with 9 wt% silicon. This is considered to be as a result of powder packing, rather than a metallurgical effect. Figures 3 and 4 show that the apparent and tap density of the bimodal powders also show a distinct peak at that constitution.

- Figures 19 and 20 plot the peak average sintered density against the apparent and tap densities of the powder mixtures. Reasonable correlation can be achieved in both cases, with the gradient of the line in Figure 20 of 1.7, suggesting that any increase in powder bed density will return, on average for these alloys, 1.7 times that increase in sintered density. This suggests that any increase in tap density which can be achieved through blending powder will have a return in terms of the quality of the finished part. However, note that the scale of this improvement does vary between the alloys. If we consider that the difference between the average sintered density and the average tap density is representative of the "densification propensity" of a particular powder blend then Figure 21 shows that this densification propensity varies, for these alloys, from 0.2 to 0.5 g/cm^3, and is only weakly correlated (correlation co-efficient 0.56) to tap density. Issues of powder bed density, metallurgy and the make-up of the blend are clearly inter-related.

Looking at the scale of these competing effects we can say, for this alloy and within the practical boundaries of this piece of work, that:

- Adding 9-12% of Si to pure Al powder (either in a powder blend or in a pre-alloyed powder) increases the sintered density by 0.5-0.6 g/cm³ (from Figure 6).

- Processing Al-Si powders and powder blends with 9-12% of Si (all the blends except III) with the processing conditions shown for Figure 7 gives an average maximum increase in sintered density over the tap density of around 0.4 g/cm³.

- The difference between sintered density and tap density for Al-Si powders and powder blends with 9-12% of Si (all the blends except III) varied between 0.25 and 0.5 g/cm³ (from Figure 21), with no strong correlation to tap density.

Clearly these competing factors are not truly separable, but the points above show that they are all, taken at the extremes of the behaviour observed in this study, important. In practical terms this would suggest that when developing processing conditions for a new alloy, an efficient approach would be to firstly develop the right processing conditions for the particular alloy and then, secondly, to optimise the bed density to attempt to increase the sintered density.

4.3 Microstructure

Figures 15-18 all show the behaviour of blend II to be somewhat different to that of the other powder blends. Blend II showed the largest fraction of primary dendrite phase and the lowest secondary dendritic arm spacing, which taken together suggest that this blend has, when processed, produced more liquid phase than the other blends, and has cooled quicker. Both of these indicate higher thermal conductivity, and this is further indicated by the fine dendritic structure at the top of the processed layers of this blend which indicates higher thermal conductivity. This would be expected for this blend when compared to the other bimodal blends on the basis of it's higher tap density – thermal conductivity is very sensitive to density variations and the peak seen in Figure 6 would suggest that the improved bed density has caused improved absorption of the laser energy, giving more liquid phase, which drives greater densification, which allows cooling to happen more quickly giving a finer microstructure. It is not clear, however, why the trimodal blends have not responded in the same way. The most obvious difference between blend II and blends VII to X

is that blends VII to X contain a proportion of the AL-4 material, and it is considered that, for this smaller sized particle, the oxide layer may have played a bigger part in determining the processing behaviour than for larger particles. Niu and Chang (2000) observed a similar effect when processing M2 HSS powders. Figures 13 and 15 suggest that some of the smaller particles in blends VII to X have remained intact throughout the process, something which could be a result of the oxide film on these particles not being ruptured. This would then disrupt the melt pool as wetting and densification would be inhibited, resulting in a poorer microstructure as thermal conductivity would also be inhibited by the oxide film covered particles. However, this requires further investigation to confirm the mechanism.

5.0 Conclusions

1. The specific laser energy input, alloy formulation and bed density have all been shown to have a significant effect of the densification of Al-Si powders and powder blends using laser sintering.

2. For a particular powder blend sintered density rose with specific laser energy input until a saturation point was reached (in this case around 125 J/mm³) beyond which increases in laser energy input did not produce further increases in density.

3. The addition of 9-12 wt% Si, either in a powder blend or in a pre-alloyed powder, to Al has a significant effect on the propensity of the resulting alloy to densify when being processed by SLS.

4. The 5:2:1 particle diameter ratio from close packed sphere analysis is a useful guide to selecting powder sizes in powder blends where high apparent or tap density is the goal. The associated 74:5:2 wt% ratio, however, has in this work underestimated the amount of the smaller particle sizes which should be used. The best results achieved in this study used a 75:20:5 wt% ratio (with 75:25 wt% almost as good), however this is likely to be influenced by the range of particle sizes, range of particle shapes, and the surface properties for a particular application.

5. Oxidation of smaller metal powders can inhibit their value in powder blends for laser sintering to a greater degree than that of larger powders. We consider it most likely that this is a result of the oxide layer being more difficult to rupture in smaller particles.

Acknowledgement

References

Bertol, L. S., Júnior, W. K., da Silva, F. P., and Aumund-Kopp, C. (2010). "Medical design: Direct metal laser sintering of Ti–6Al–4V." Materials & Design, (Article in Press)

Callister, W. D. (2007). Materials Science and Engineering: An Introduction. New York, John Willey & Sons, Inc.

Dinsdale, A. T., and Quested, P. N. (2004). "The viscosity of aluminium and its alloys - A review of data and models." Journal of Materials Science **39**(24): pp. 7221-7228.

German, R. M. (1996). Sintering Theory and Practice. New York, John Wiley & Sons, Inc.

Gokhale, A. M. (2004) in *ASM Handbook: Metallography, and Microstructures,* edited by Vander Voort G. F. & Lampman, S. (ASM International, Materials Park, OH), 2004, 428.

Gunduz, M., and Cardirli, E. (2002). "Directional solidification of aluminium-copper alloys." Materials Science and Engineering A. **327**: pp.167-185.

Hauser, C. (2003). Selective Laser Sintering of a Stainless Steel Powder School of Mechanical Engineering Leeds, University of Leeds **PhD:** p.1-270.

MPIF (1995). Standard Test Methods for Metal Powders and Powder Metallurgy

Products. Princeton, New Jersey., Metal Powder Industries Federation.

Mumtaz, K. A., Erasenthiran, P., and Hopkinson, N. (2008). "High density selective laser melting of Waspaloy." Journal of Materials Processing Technology, **195**(1-3), pp. 77-87

Nakamoto, T., Shirakawa, N., Miyata, Y., and Inui, H. (2009). "Selective laser sintering of high carbon steel powders studied as a function of carbon content." Journal of Materials Processing Technology, **209**(15-16), pp. 5653-5660

Niu, H. J. and Chang., I.T.H. (2000). "Selective laser sintering of gas atomized M2 high speed steel powder." Journal of Materials Science **35**: pp.31-38.

Olakanmi, E. O. (2008) Direct selective laser sintering of aluminium alloy powders Institute for Materials Research, Leeds, University of Leeds **PhD:** p.1-378.

Simchi, A. (2006). "Direct laser sintering of metal powders: Mechanism, kinetics and microstructural features." Materials Science and Engineering A. **428**(1-2): pp.148-158.

Zhu, H. H., Fuh, J. Y. H., and Lu, L. (2007). "The influence of powder apparent density on the density in direct laser-sintered metallic parts." International Journal of Machine Tools and Manufacture **47**(2): pp.294-298.

Material properties and laser sintered behaviour of hypoeutectic Al-Si powders.
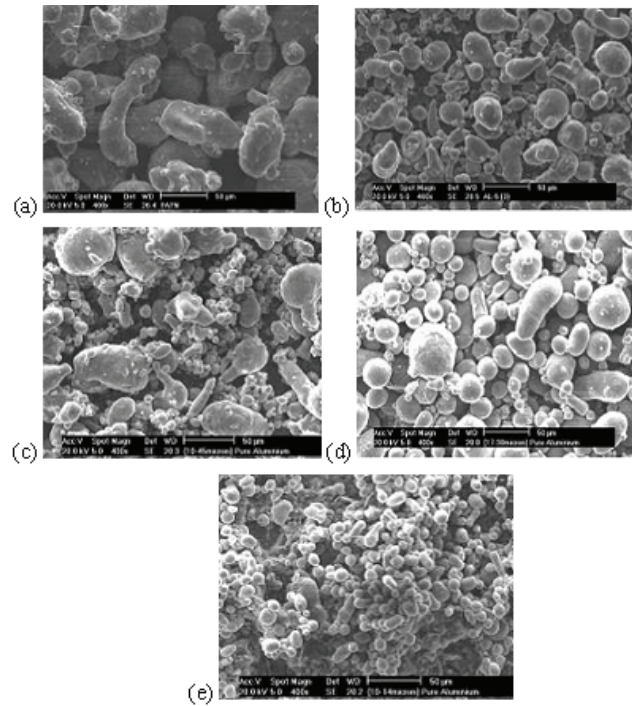
Figure 1: SEM images of powders: (a) 45-75 micron (AL-1); (b) 45-75 micron (Al-12Si); (c) 10-45 micron (AL-2); (d) 17-30 micron (AL-3); (e) 10-14 micron (AL-4) powders.
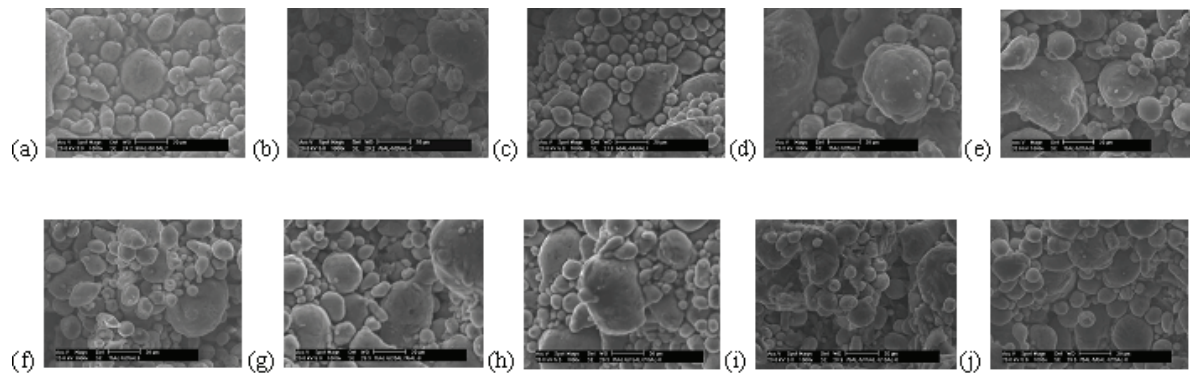
Figure 2: SEM images of blended powders: (a) I (b) II (c) III (d) IV (e) V (f) VI (g) VII (h) VIII (i) IX (j) X.
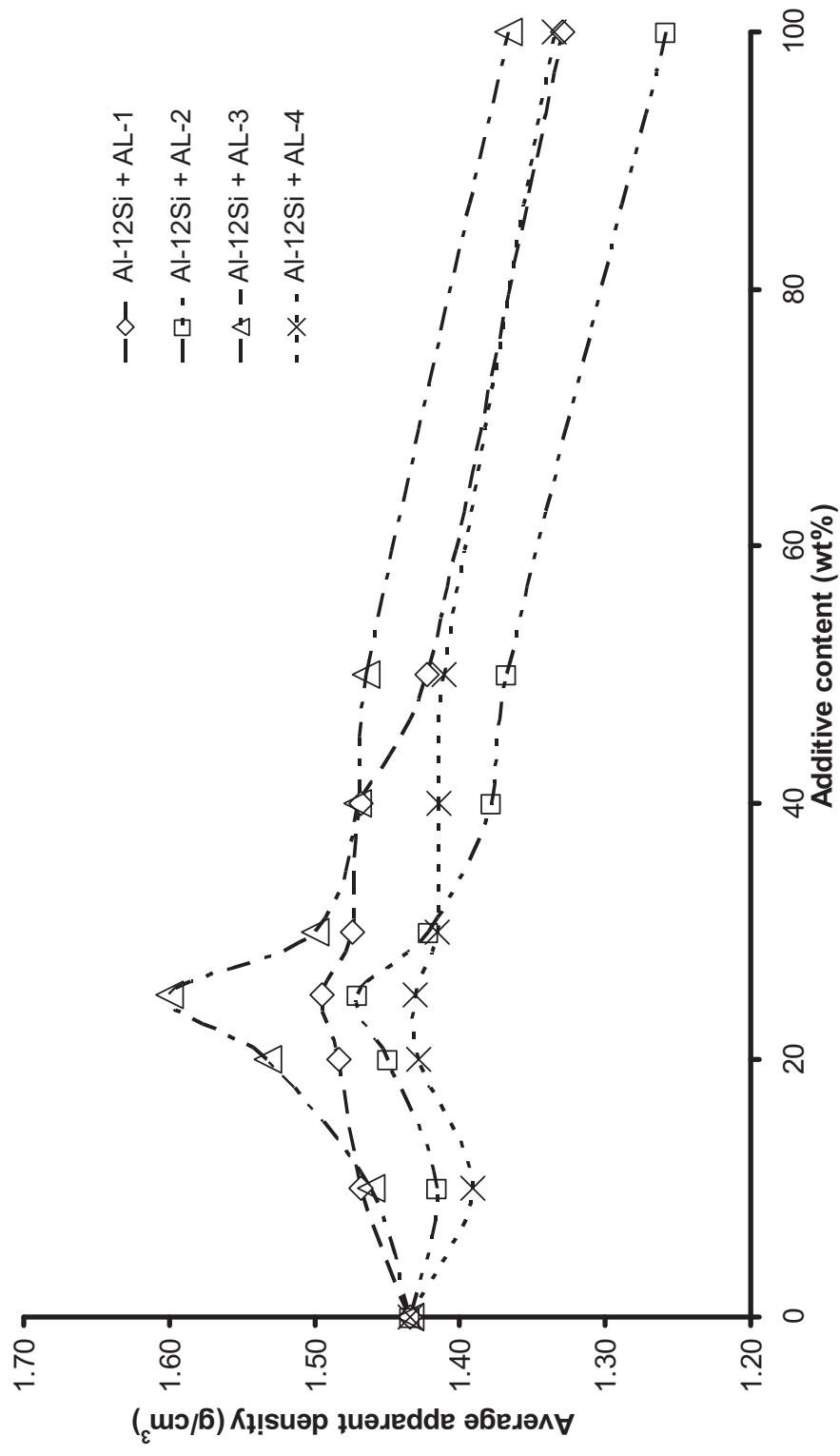
**Figure 3: Effect of varying additive level on the apparent density of bimodal powders.**
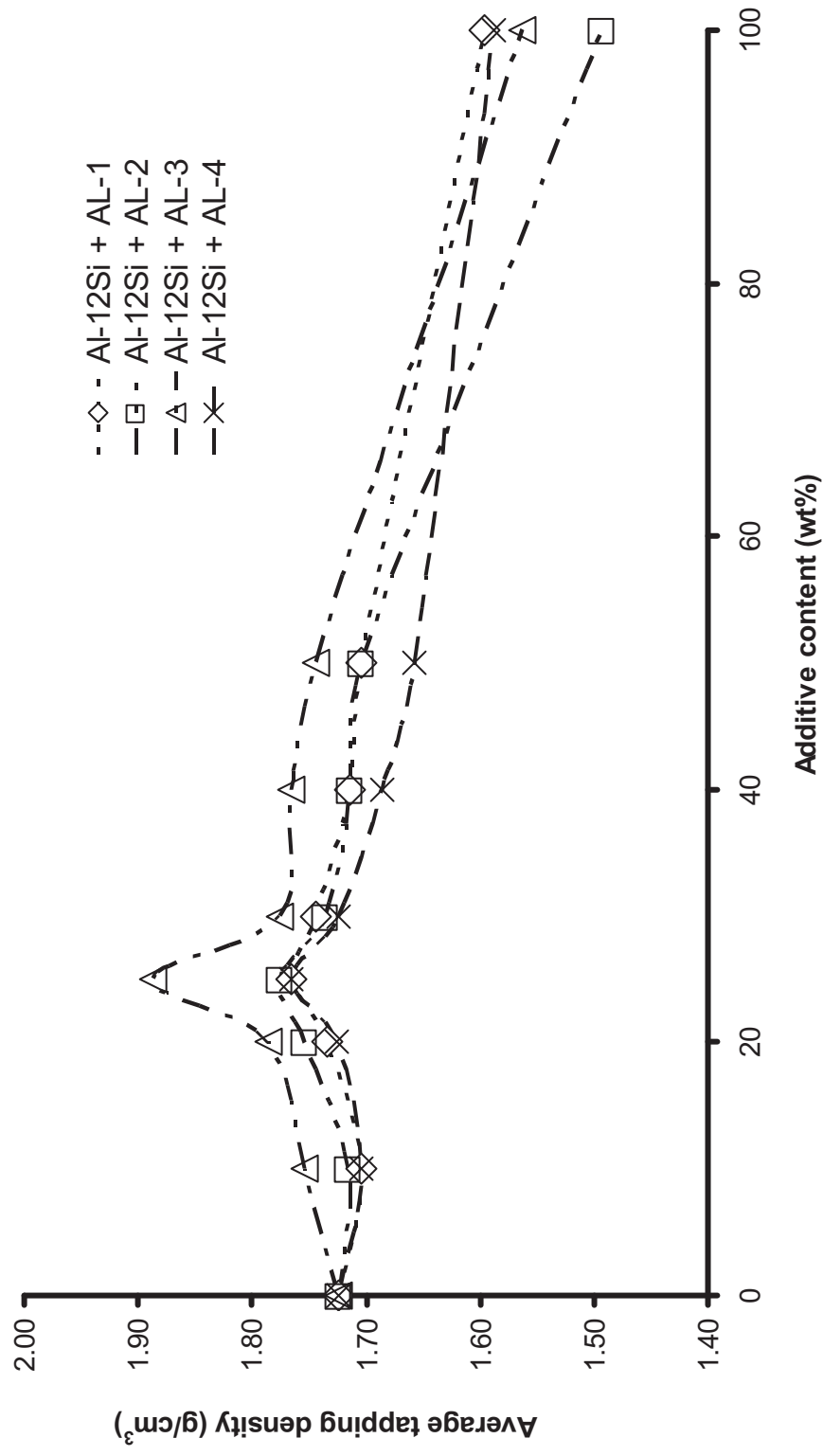
Figure 4: Effect of varying additive level on the tapping density of bimodal powders
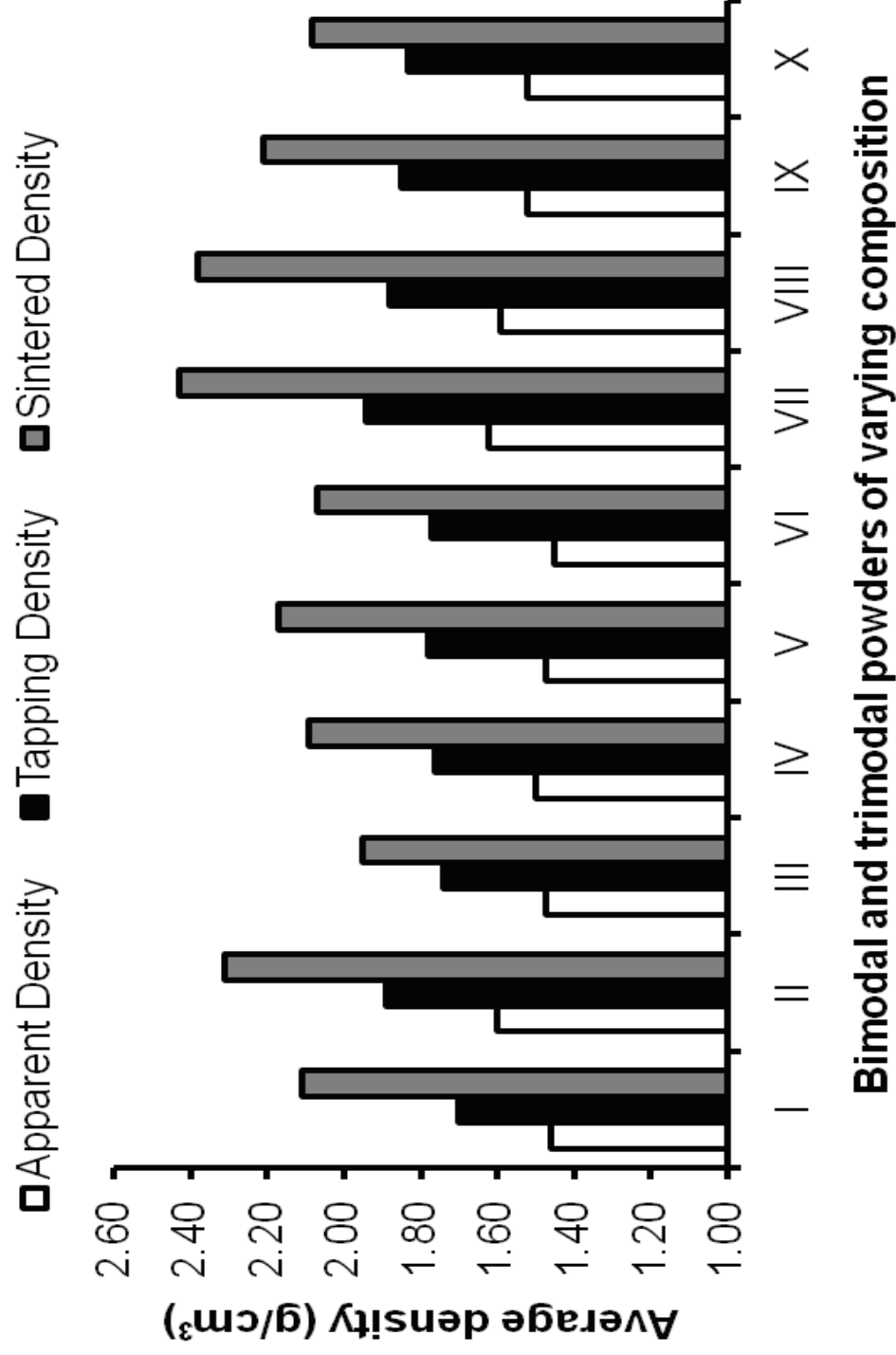
Figure 5: Comparison of the apparent, tapping, and sintered densities (laser power of 200 W, scan speed of 65 mm/s, layer thickness of 0.25mm, and a scan spacing of 0.1 mm) of bimodal with trimodal powders.
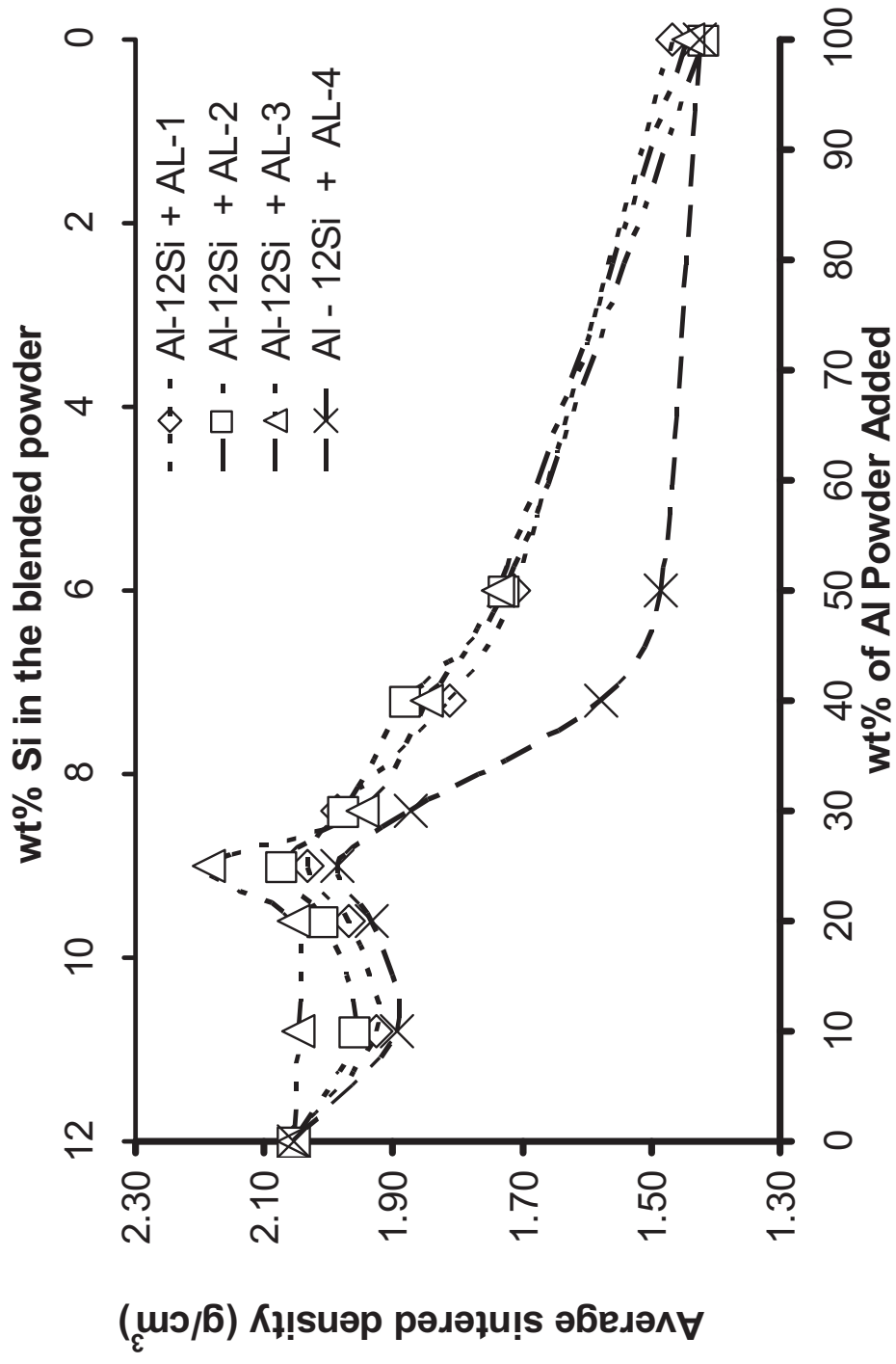
Figure 6: Effect of pure Al powder content and silicon constitution on the sintered density of SLS processed blended powders. Laser power 200 W, scan speed 120 mm/s, layer thickness of 0.25 mm, and a scan spacing of 0.1 mm.
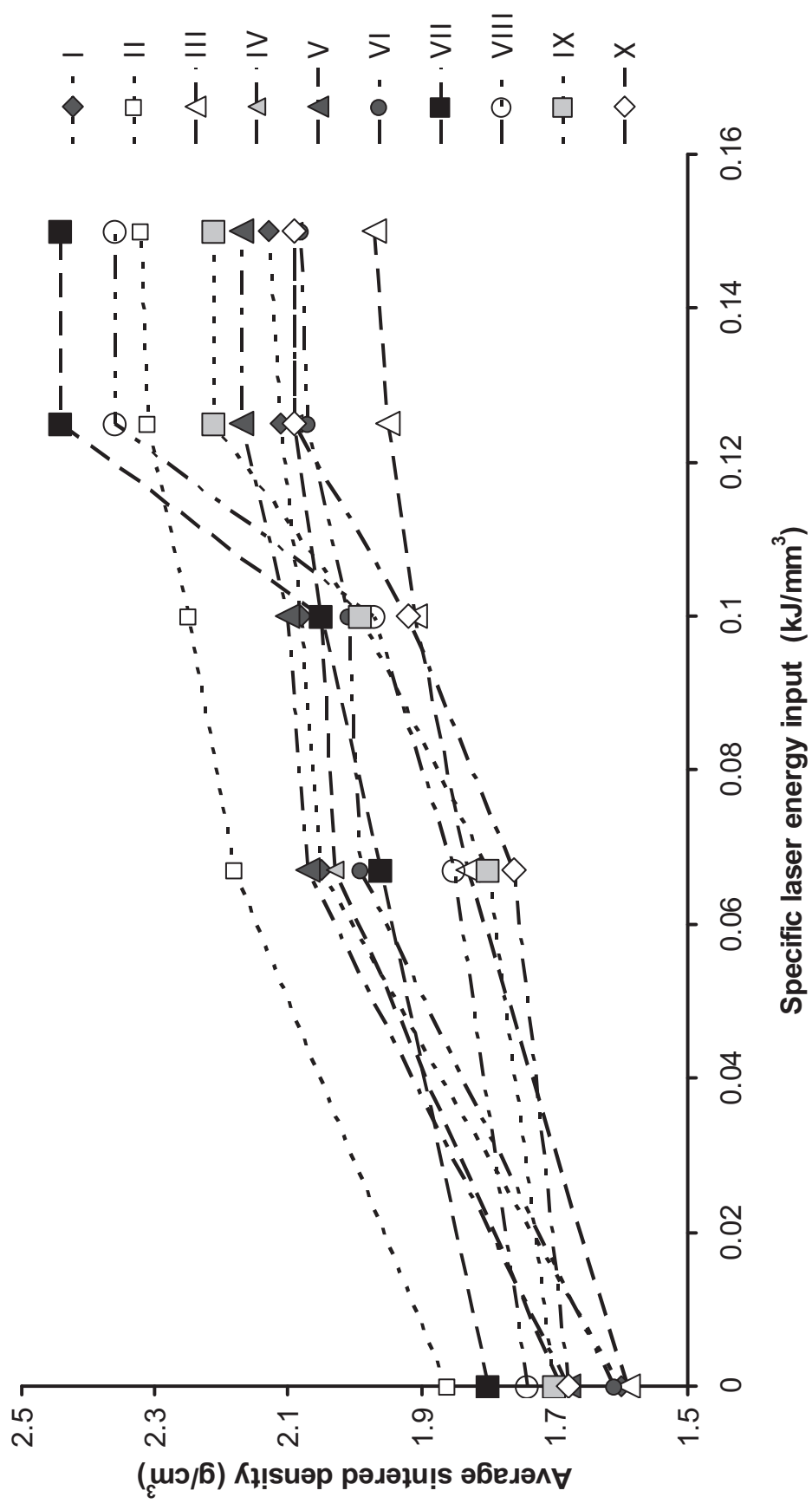
Figure 7: Relationship between the sintered density and the specific laser energy input for bimodal and trimodal powders of varying composition. Laser power 200 W, layer thickness of 0.25mm, scan spacing of 0.1 mm, and varying scan speed defined by equation 1. Points on y-axis are tap density.
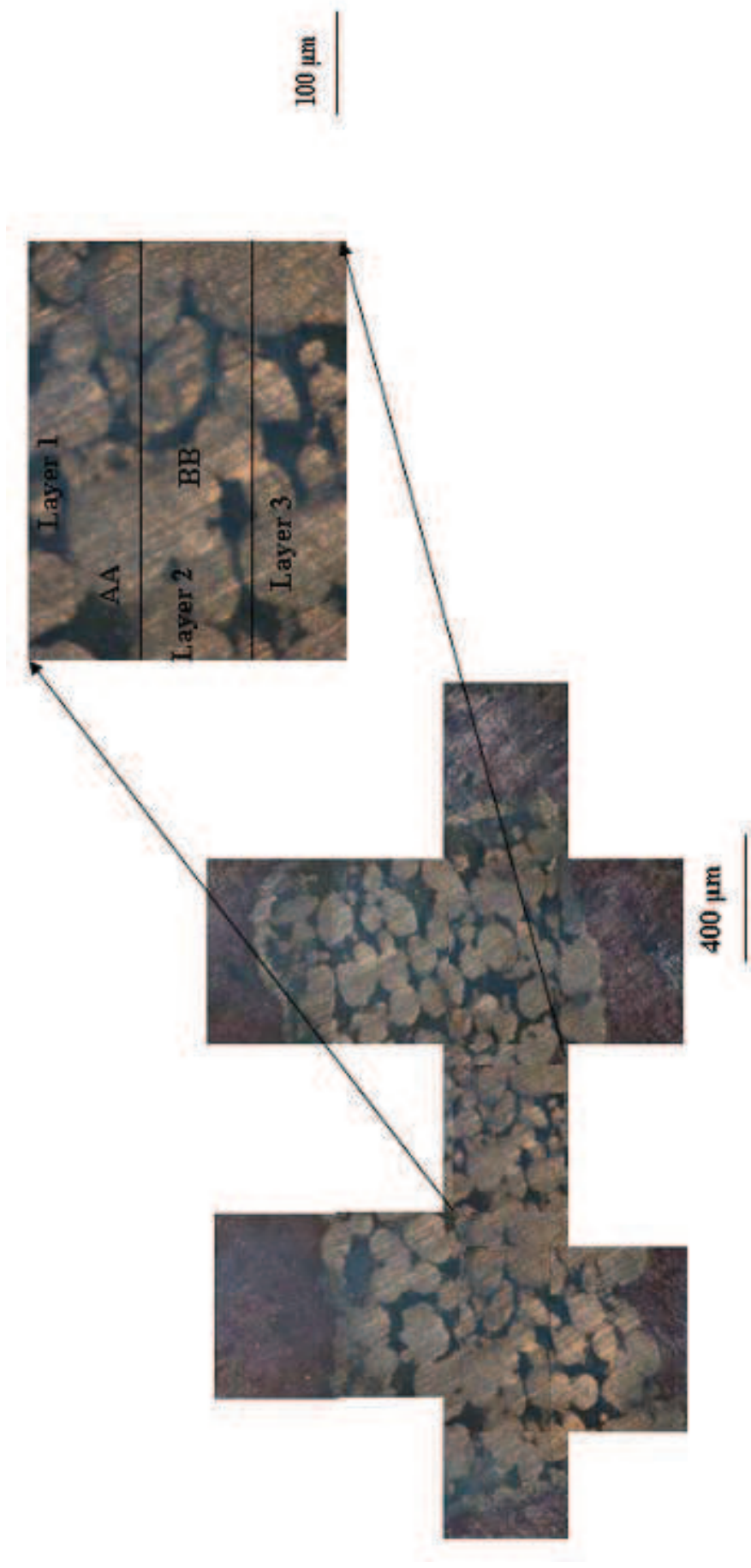
Figure 8: Sections through laser sintered Al-12Si (90wt%) - AL-3 (10wt%) blended powder. Laser power 200 W, scan speed 53 mm/s, layer thickness 0.25mm, scan spacing of 0.1 mm (specific laser energy input 150 J/mm³).
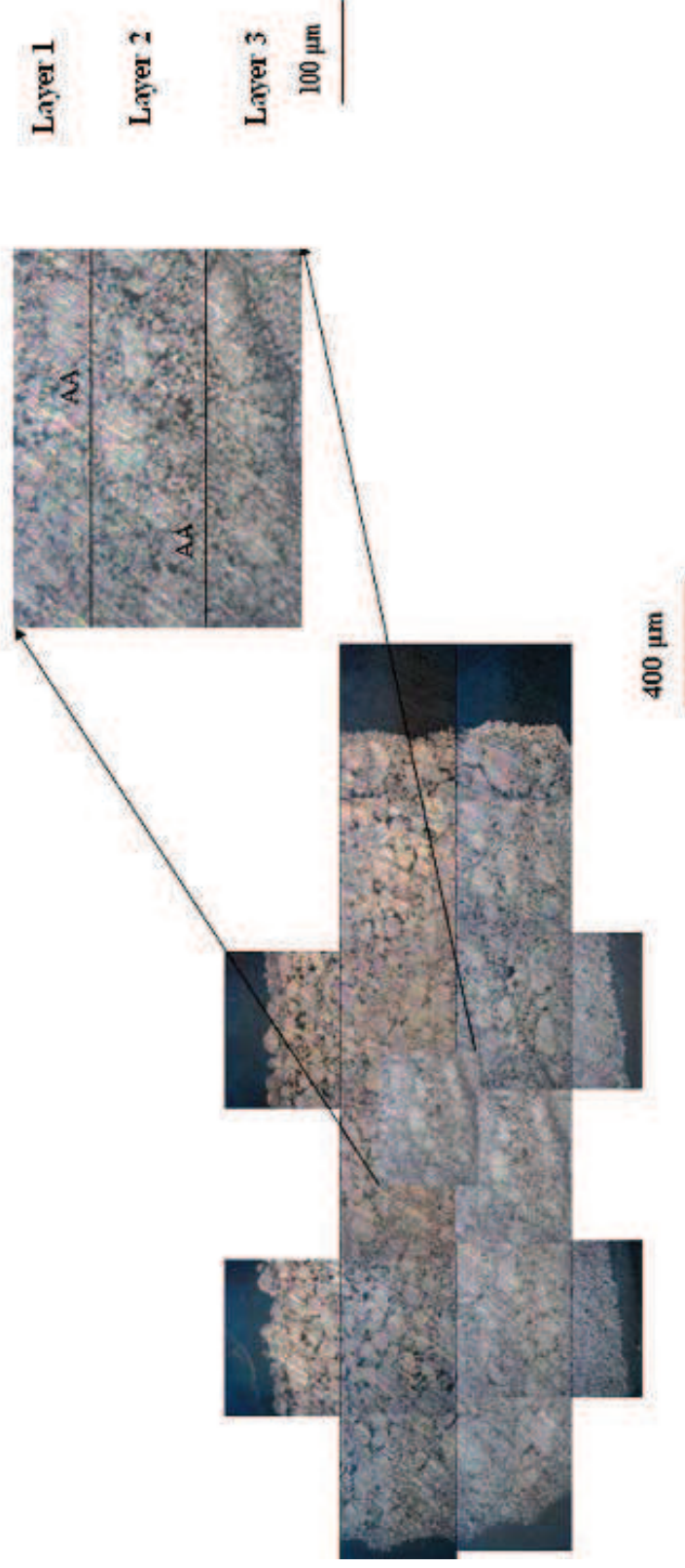
Figure 9: Sections through laser sintered Al-12Si (75wt%) - AL-3 (25wt%) blended powder. Processing conditions as Figure 8.
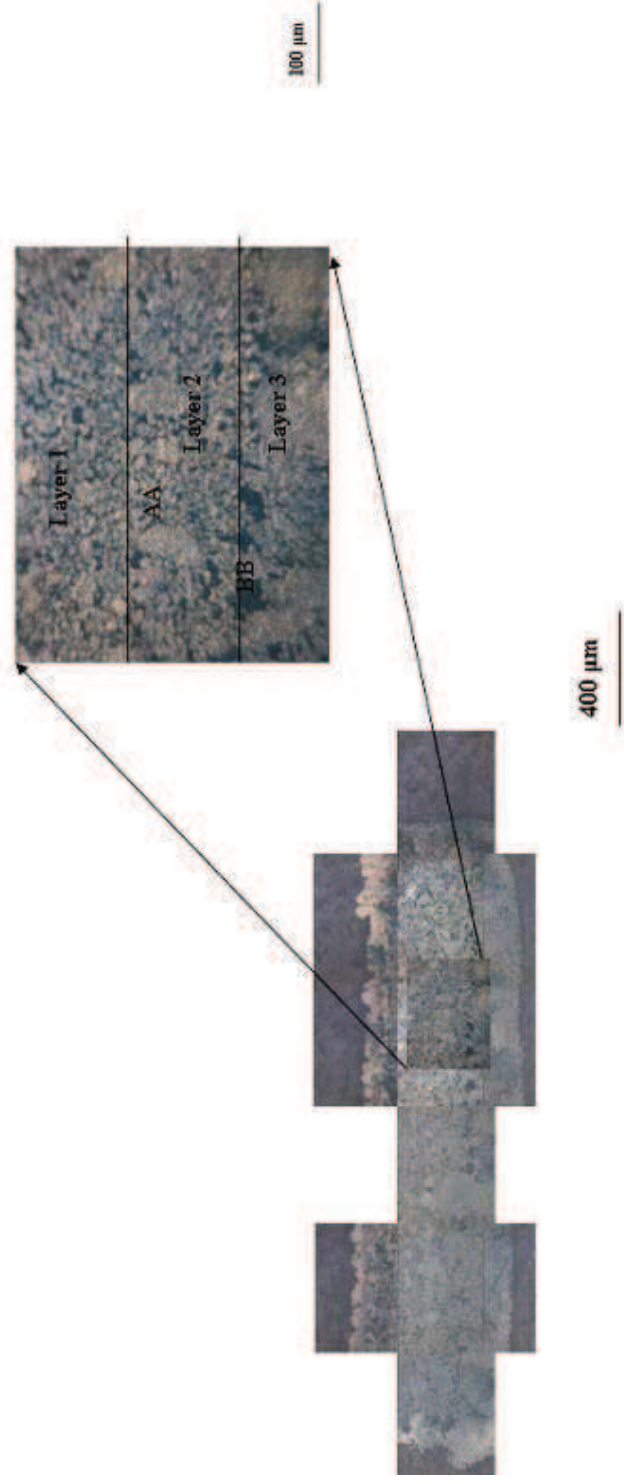
**Figure 10: Sections through laser sintered 75wt% Al-12Si - 25wt% AL-4 blended powder. Processing conditions as Figure 8.**
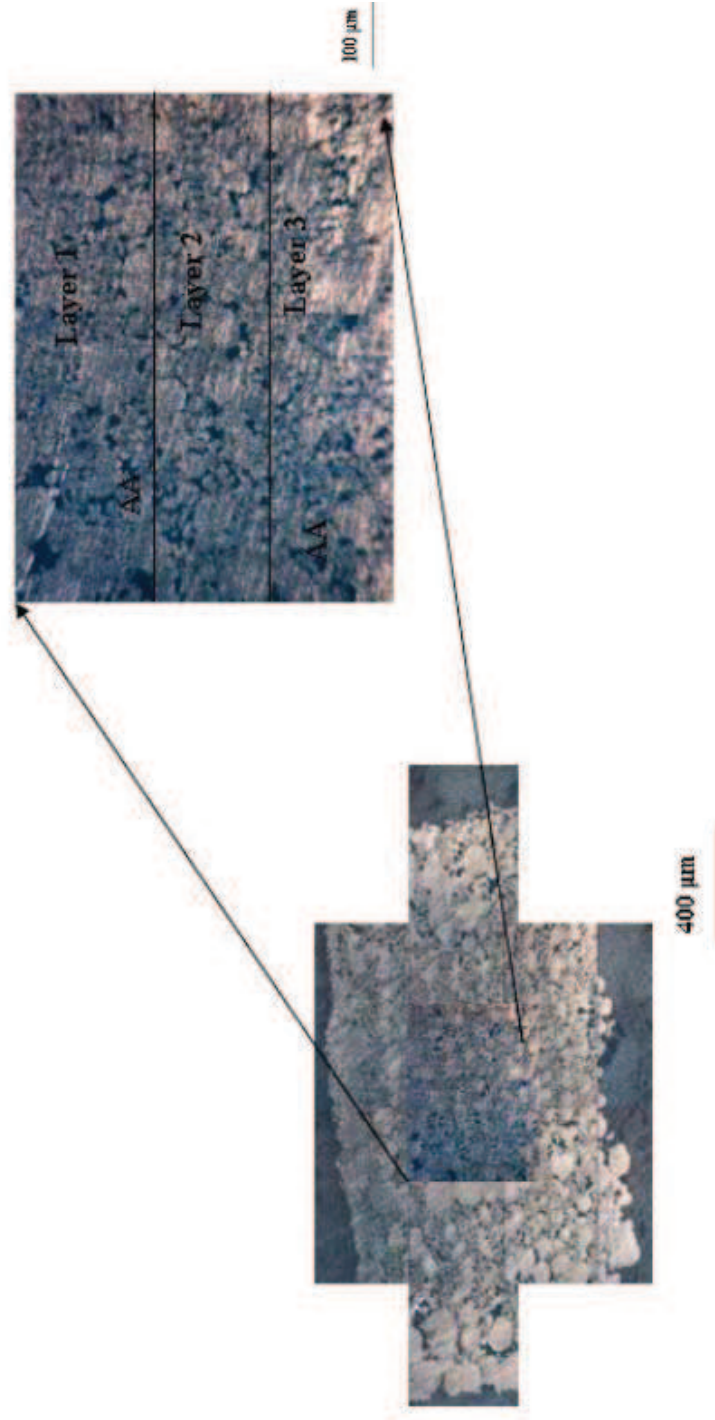
Figure 11: Microstructure of sections through 75wt% Al-12Si-20wt% AL-3 – 5wt% AL-4. Processing conditions as Figure 8.
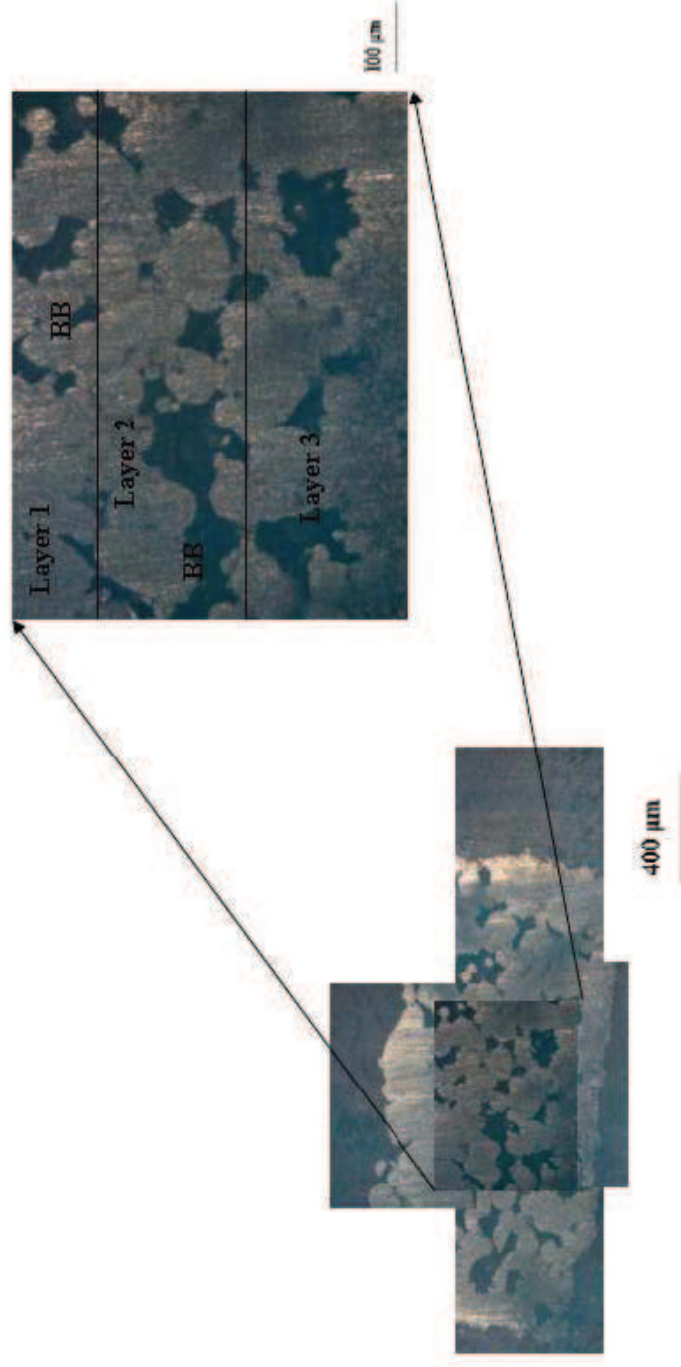
Figure 12: Microstructure of sections through 75wt% Al-12Si - 5wt% AL-3 - 20wt% AL-4. Processing conditions as Figure 8.
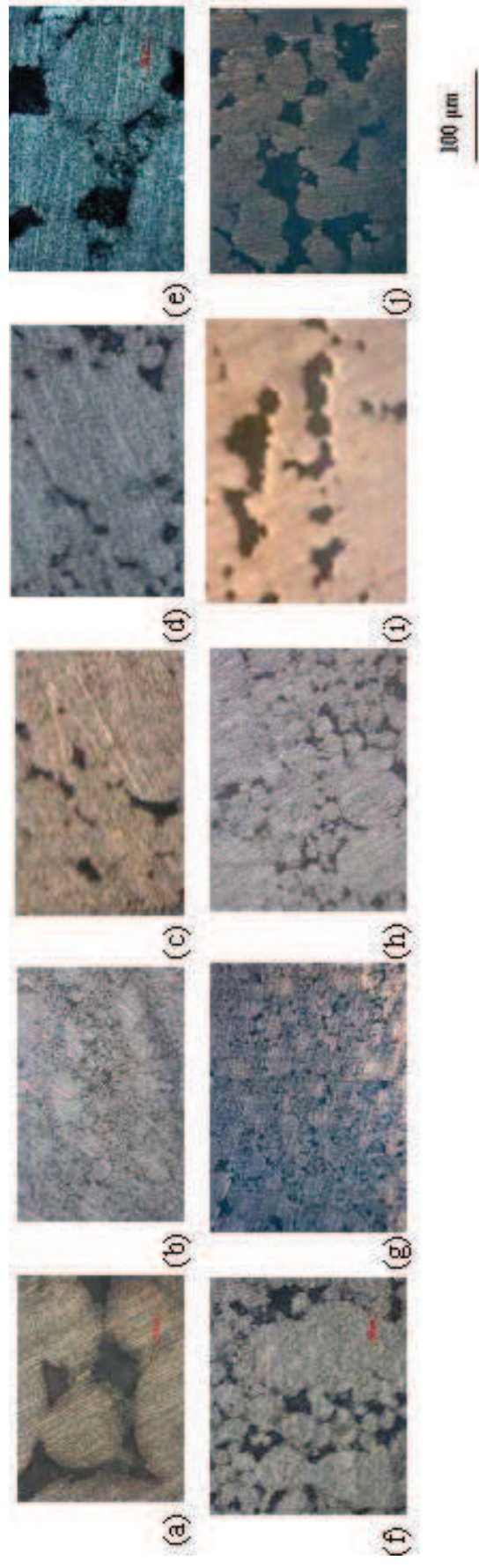
Figure 13: Optical microscopy images of characteristic microstructures of laser sintered bimodal and trimodal powders: (a) I (b) II (c) III (d) IV (e) V (f) VI (g) VII (h) VIII (i) IX (j) X.
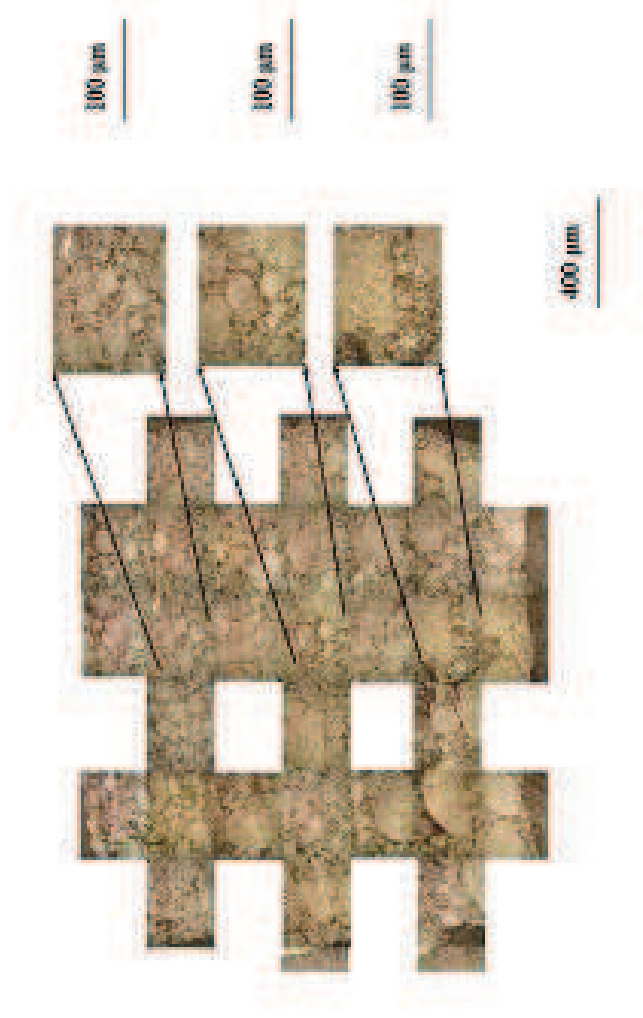
Figure 14: Sections through the micrograph of laser sintered Al-12Si powder. Laser powers 200 W, scan speed 120 mm/s, layer thickness 0.25mm, scan spacing of 0.1 mm (specific laser energy input of 67 J/mm³).
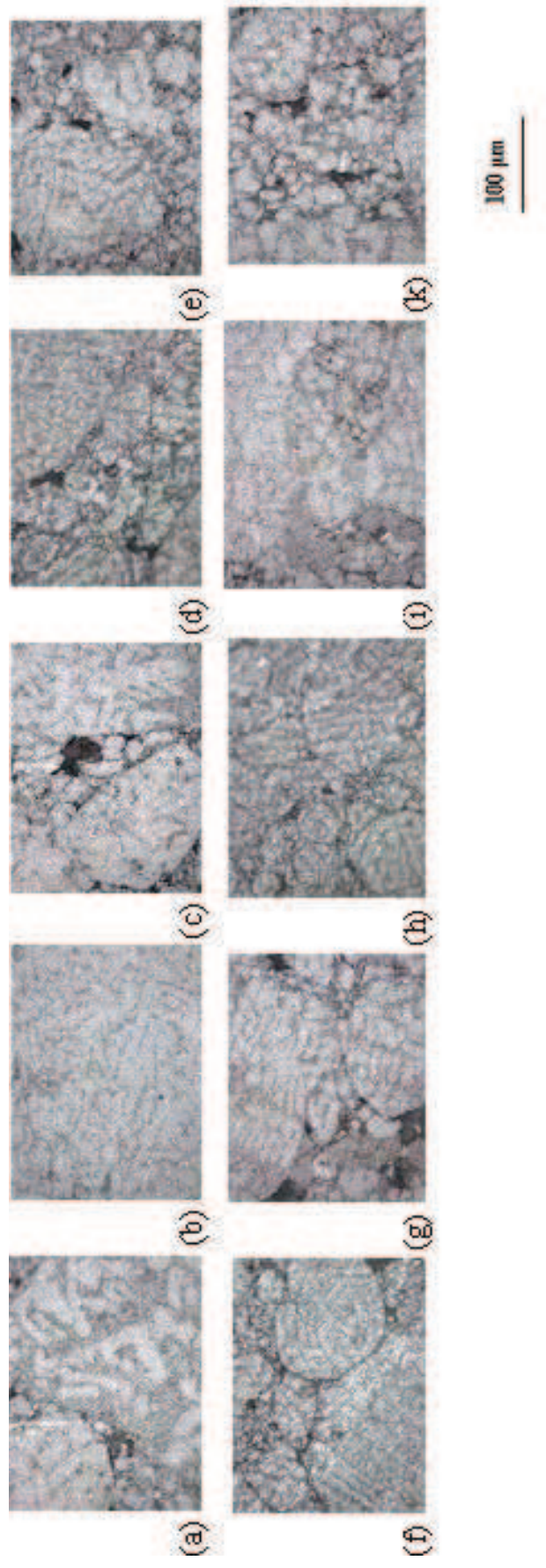
Figure 15: Microstructural heterogeneity and homogeneity in SLS processed bimodal and trimodal powders: (a) I (b) II (c) III (d) IV (e) V (f) VI (g) VII (h) VIII (i) IX (j) X.
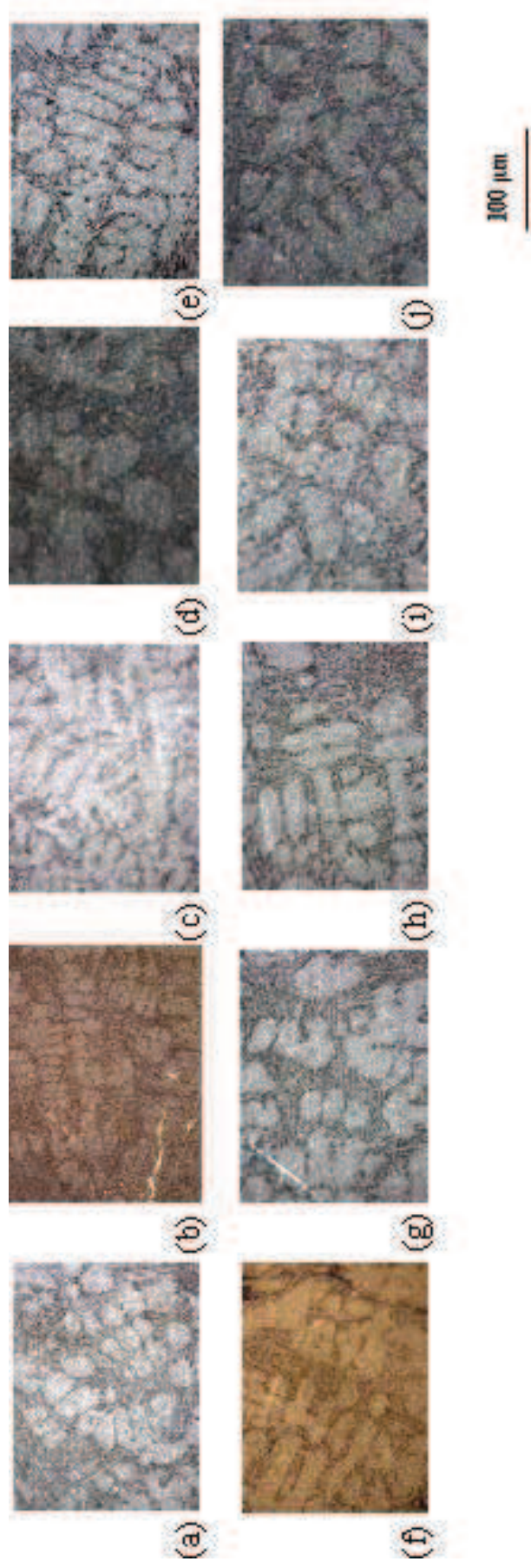
Figure 16: The nature of dendritic microstructure discovered at the top portion of the SLS processed bimodal and trimodal powders: (a) I (b) II (c) III (d) IV (e) V (f) VI (g) VII (h) VIII (i) IX (j) X.

15

Figure 17: The nature of dendritic microstructure discovered at the bottom portion of the SLS processed bimodal and trimodal powders: (a) I (b) II (c) III (d) IV (e) V (f) VI
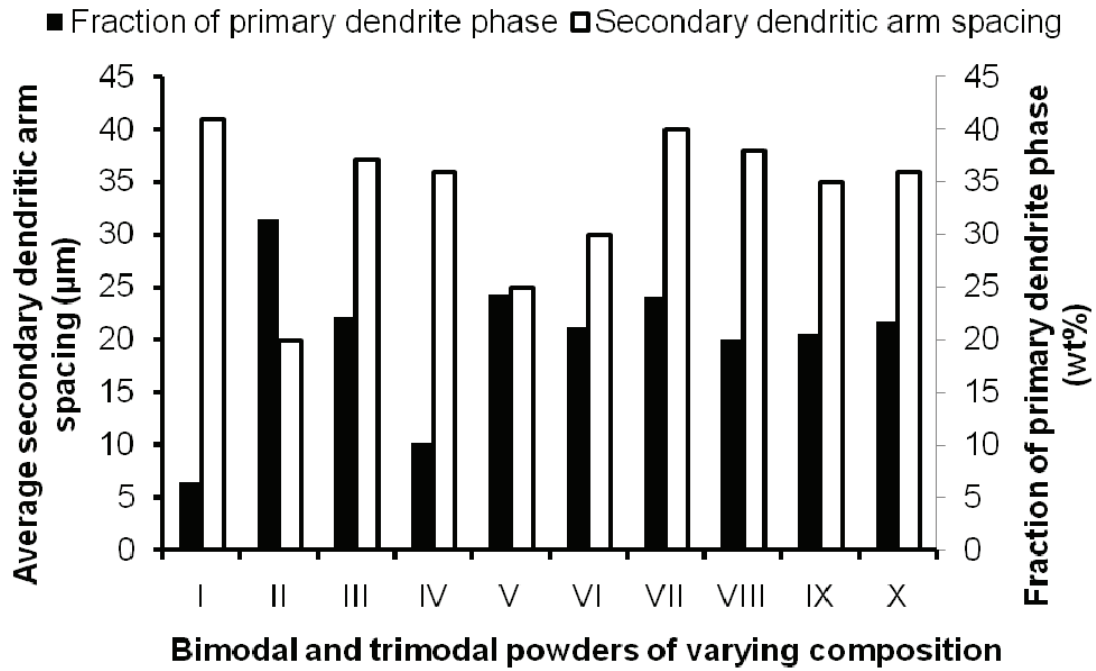
Figure 18: Comparison of the average secondary dendrite arm spacing and fraction of primary dendrite phase in SLS processed bimodal and trimodal powders.
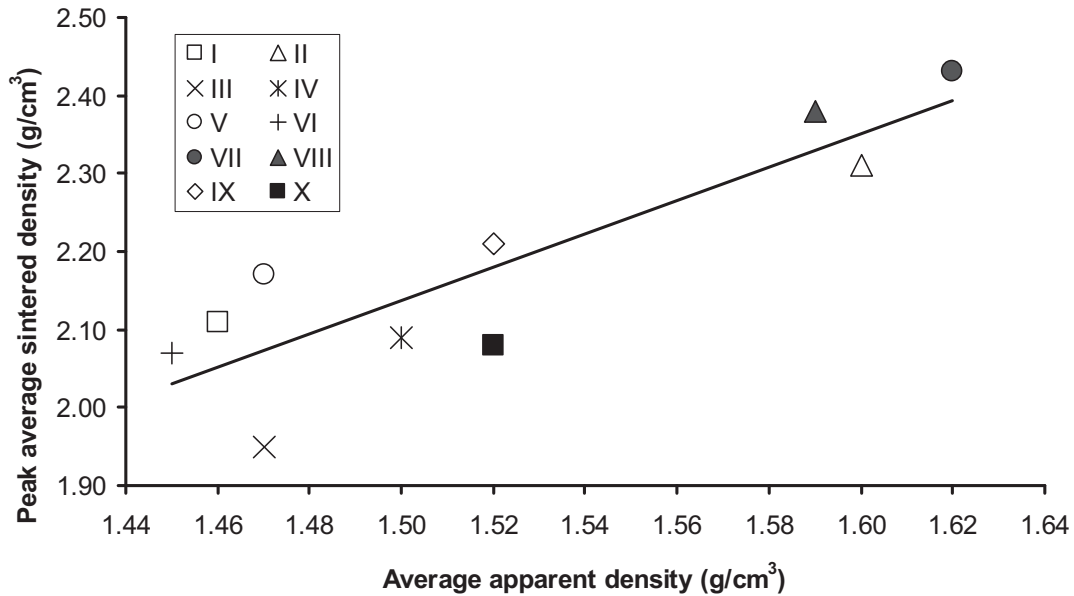

Figure 19: Relationship between the peak sintered density and bed density (correlation co-efficient = 0.77) of blended bimodal and trimodal samples fabricated using specific laser energy input of 125 J/mm^3.
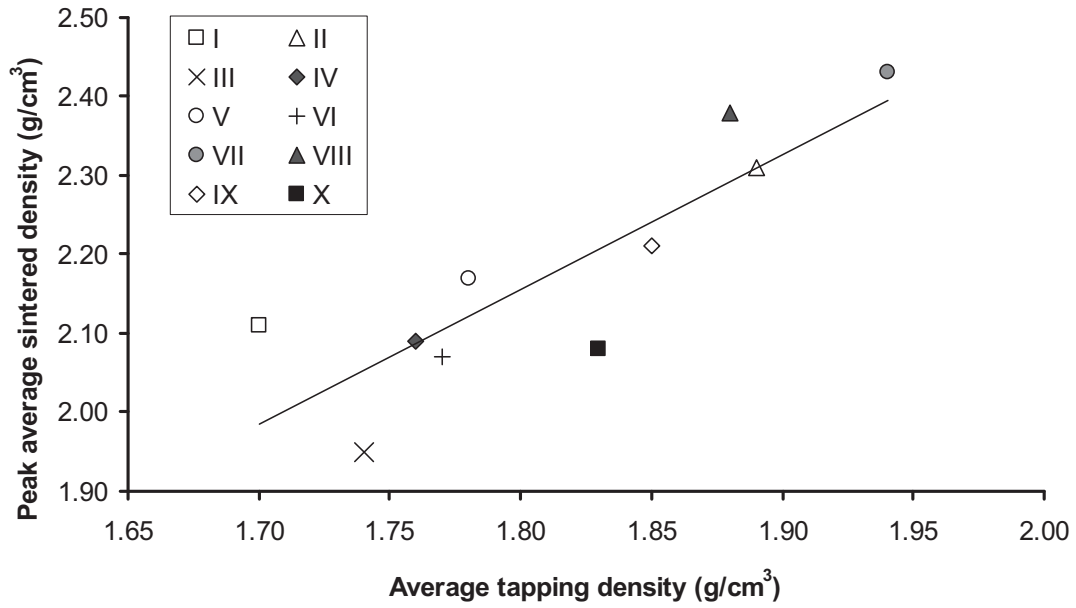
Figure 20: Relationship between the peak sintered density and tapping density (correlation co-efficient = 0.73) of blended bimodal and trimodal samples fabricated using specific laser energy input of 125 J/mm³.
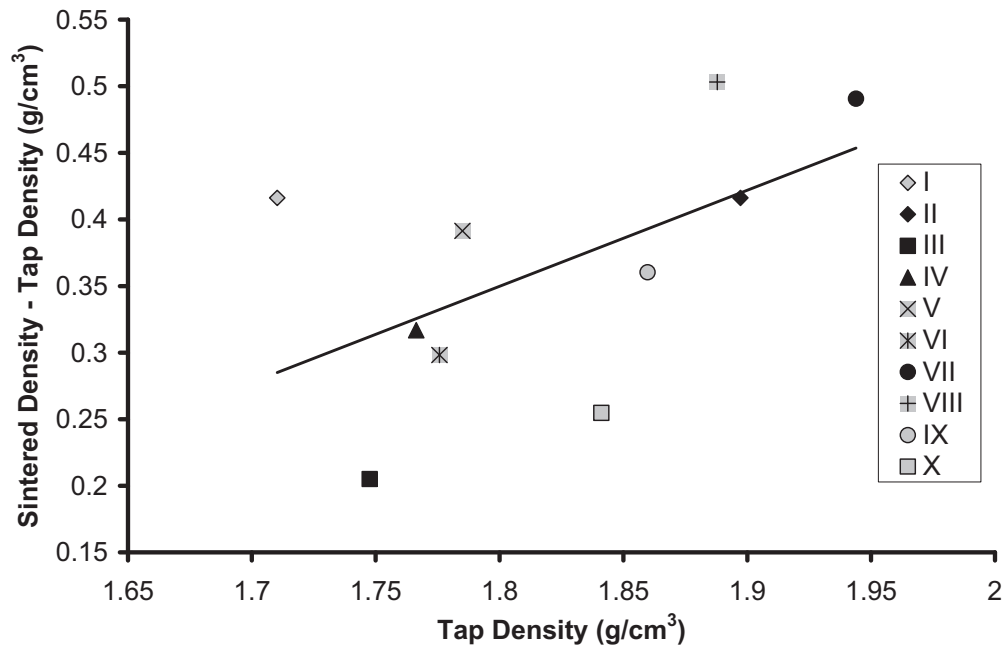

Figure 21: Relationship between the densification achieved by SLS processing (sintered density – tap density) and tapping density (correlation co-efficient = 0.56) of blended bimodal and trimodal samples fabricated using specific laser energy input of 125 J/mm³.